AIP Physics of Plasmas

Mirror force induced wave dispersion in Alfvén waves

P. A. Damiano and J. R. Johnson

Citation: Phys. Plasmas **20**, 062901 (2013); doi: 10.1063/1.4810788
View online: http://dx.doi.org/10.1063/1.4810788
View Table of Contents: http://pop.aip.org/resource/1/PHPAEN/v20/i6
Published by the American Institute of Physics.

Additional information on Phys. Plasmas

Journal Homepage: http://pop.aip.org/
Journal Information: http://pop.aip.org/about/about_the_journal
Top downloads: http://pop.aip.org/features/most_downloaded
Information for Authors: http://pop.aip.org/authors

ADVERTISEMENT

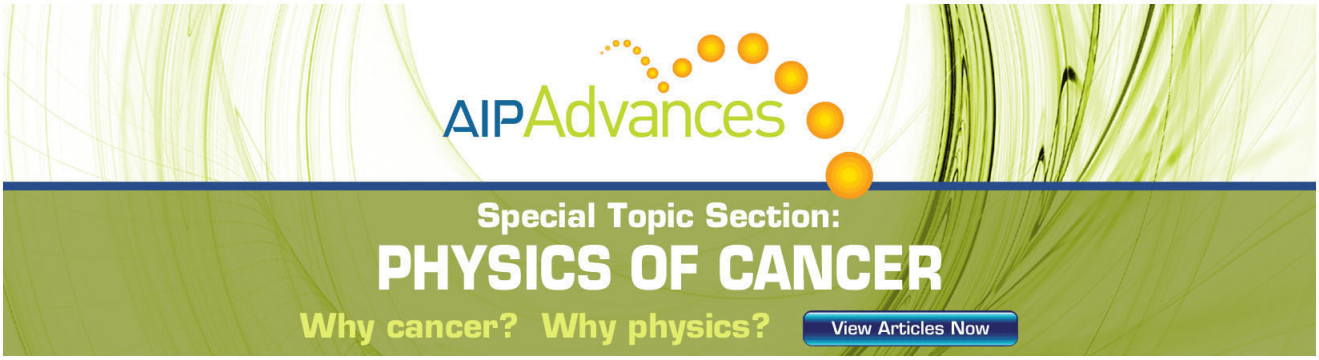

PHYSICS OF PLASMAS **20**, 062901 (2013)

Mirror force induced wave dispersion in Alfvén waves

P. A. Damiano[a)] and J. R. Johnson
Princeton Plasma Physics Laboratory, Princeton, New Jersey 08543-0451, USA

(Received 10 March 2013; accepted 30 April 2013; published online 12 June 2013)

Recent hybrid MHD-kinetic electron simulations of global scale standing shear Alfvén waves along the Earth's closed dipolar magnetic field lines show that the upward parallel current region within these waves saturates and broadens perpendicular to the ambient magnetic field and that this broadening increases with the electron temperature. Using resistive MHD simulations, with a parallel Ohm's law derived from the linear Knight relation (which expresses the current-voltage relationship along an auroral field line), we explore the nature of this broadening in the context of the increased perpendicular Poynting flux resulting from the increased parallel electric field associated with mirror force effects. This increased Poynting flux facilitates wave energy dispersion across field lines which in-turn allows for electron acceleration to carry the field aligned current on adjacent field lines. This mirror force driven dispersion can dominate over that associated with electron inertial effects for global scale waves. © *2013 AIP Publishing LLC*.
[http://dx.doi.org/10.1063/1.4810788]

I. INTRODUCTION

Field Line Resonances (FLRs) are ultra low frequency (mHz) standing shear Alfvén wave structures that form along the Earth's closed dipolar magnetic field lines and typically result from mode conversion of fast compressional modes. These standing waves have been linked to the formation of some discrete auroral arcs [e.g., Refs. 1–3]. In order to understand how electrons are accelerated to sufficient energies within these waves to drive auroral emissions, a number of studies, including both theoretical[4–6] and simulations,[7–9] have looked to mirror force effects as a candidate to account for the keV potential drops needed to accelerate electrons to sufficient energies to explain the auroral emissions. References 8 and 9 considered the upward current region (corresponding to the downward propagation of magnetospheric electrons) of a toroidal standing shear Alfvén wave system using a 2-D hybrid MHD-kinetic electron model in dipolar coordinates for a constant resonance width and a range of electron thermal temperatures from 5 eV to a keV. A saturation and broadening of parallel current profile perpendicular to the magnetic field was noted that was enhanced by a depletion of electrons at small pitch angles. The magnitude of the broadening was found to increase substantially with the temperature of the electron distribution function. Fundamentally, a perpendicular dispersion of wave energy should result when there is a cross-field component to the Poynting flux, which occurs when there is a parallel component of the electric field. This dispersion is well known in the context of electron inertial or kinetic Alfvén waves [e.g., Ref. 10], but has not been addressed in the context of a mirror kinetic Alfvén wave (to borrow the terminology of Reference 5). In order to understand if mirror force effects on the parallel electric field can account for the broadening evident in these aforementioned kinetic simulations, in the present study we consider a simplified MHD description that incorporates a resistive parallel Ohm's law ($j_{||} = \sigma_{||} E_{||}$) where $\sigma_{||}$ is determined from the linear version of the Knight relation[11] (which describes the mirror force driven current-voltage relation along an auroral field for a static potential drop). This simplified analysis allows us to separate out the effects of the complicated wave-particle interactions evident in the hybrid simulations and focus on the effects of $E_{||}$ alone.

II. DESCRIPTION OF MODELS

A. Hybrid and MHD models

Two models will be utilized in the present study. The first is a 2D hybrid MHD kinetic-electron model in dipolar coordinates presented initially in Reference 7. The dipolar model geometry is presented in Figure 1 where the x_1 (magnetic field-aligned) and x_2 (radial) directions are explicitly included in the simulation domain. The system is independent of the azimuthal coordinate so that $\partial/\partial x_3 = 0$ and incorporates only azimuthal components for the plasma bulk velocity (u_3) and magnetic field (b_3) described by the linearized cold plasma MHD momentum equation and Faraday's law in curvilinear coordinates given respectively by

$$\mu_o \rho_o \frac{\partial u_3}{\partial t} = \frac{B_o}{h_1 h_3}\left(\frac{\partial}{\partial x_1}(h_3 b_3)\right), \tag{1}$$

$$\frac{\partial b_3}{\partial t} = \frac{-1}{h_1 h_2}\left(\frac{\partial}{\partial x_1}(h_2 E_2) - \frac{\partial}{\partial x_2}(h_1 E_1)\right), \tag{2}$$

with the perpendicular Ohm's Law,

$$E_2 = -u_3 B_o, \tag{3}$$

where B_o is the magnitude of the ambient dipolar magnetic field; E_1 and E_2 are the parallel and radial components of the electric field; $x_1 = \cos\theta/r^2, x_2 = \sin^2\theta/r, x_3 = \phi$ and h_1, h_2,

[a)]Electronic mail: pdamiano@pppl.gov

 © 2013 AIP Publishing LLC

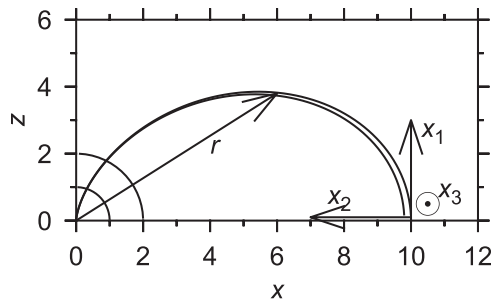

FIG. 1. Simulation domain (from Ref. 7) where x_3 is positive increasing out of the page (only upper half plane shown). The circles of radius 1 and 2 R_E respectively denote the surface of the Earth and "ionospheric" boundary. The angle θ is subtended from the z axis. Perpendicular boundaries are at the L = 9.4 and L = 10 field lines where L is the standard McIlwain parameter denoting the distance of the field line from the center of the Earth in the magnetic equatorial plane (z = 0 axis) measured in R_E.

and h_3 are the dipolar metrics [e.g., see Ref. 7]. Equations (1) to (3) are solved on set model grid points and are coupled to a system of kinetic electrons that are free to move anywhere in the simulation domain following the guiding center equations for the parallel electron dynamics given by

$$m_e \frac{dv_1}{dt} = -eE_1 - \mu_m \frac{1}{h_1}\frac{\partial B_o}{\partial x_1}, \tag{4}$$

$$h_1 \frac{dx_1}{dt} = v_1, \tag{5}$$

where v_1 is the parallel electron velocity and $\mu_m = m_e v_\perp^2/(2B)$ is the magnetic moment. Equations (1)–(3) with $E_1 = 0$, provide a self-consistent linear model of Alfvén wave propagation where massless electrons respond to ion polarization currents perpendicular to the ambient magnetic field in order to maintain quasineutrality. The MHD and kinetic portions of the model are closed via the algorithm for the parallel electric field which incorporates the generalized Ohm's law (including electron inertia, electron pressure, and mirror force contributions) and an auxiliary Poisson's equation in terms of the current density for the enforcement of quasineutrality.[7] Standard Particle-In-Cell techniques are used to calculate the moments of the electron distribution function and interpolate the field values to the particle positions.

The results of the kinetic model are compared with an MHD description incorporating Eqs. (1)–(3) along with a simple parallel Ohm's law given by $E_{||} = E_1 = (1/\sigma)j_1$ where we will consider the current saturation and broadening in the ideal case ($E_1 = 0$) and for cases where constant values of σ are chosen based on the linear version of the Knight relation[11] for the same electron temperatures and densities.

III. SIMULATIONS

In order to interpret the current broadening seen in References 8 and 9, the simulations are initialized in the same manner by perturbing the azimuthal fluid velocity in Eq. (1) using an approximate eignemode solution of the fundamental standing mode along an L = 10 magnetic field line. Perpendicular to the magnetic field, the initial perturbation has a 1/2 Gaussian profile that allows for the consideration of only an upward current region corresponding to the downward acceleration of magnetospheric electrons. The Full Width Half Maximum of the perpendicular Gaussian profile at the equator was 0.5 R_E. Correspondingly, the electrons are initialized as a Maxwellian with an empty loss cone (see Ref. 8 for complete details) and are positioned to form a constant density profile everywhere ($n_e = n_i = 1\,\mathrm{cm}^{-3}$ which yields $\lambda_e \approx 5$ km and an Alfvén period for the mode of $T_A = 270$ s). Although this initialization neglects the mode conversion process that leads to the formation of the resonance, it provides a framework to understand how electrons respond to the wave perturbation in the upward current phase of the resulting standing mode. The initialization of the electrons is also consistent with only perturbing the initial u_ϕ because there are no initial currents within the system.

Figure 2 displays the hybrid model parallel current density, j_1, at the northern ionospheric boundary (corresponding to the hemisphere displayed in Fig. 1) for electron temperatures of 200 eV (Figure 2(a)) and 1 keV (Figure 2(b)) at two different times. Superimposed on the hybrid model results is the corresponding ideal MHD solution ($E_1 = 0$) at the later time ($t = 0.2\ T_A$). The parallel current, j_1 grows with time but then eventually saturates and broadens relative to the MHD

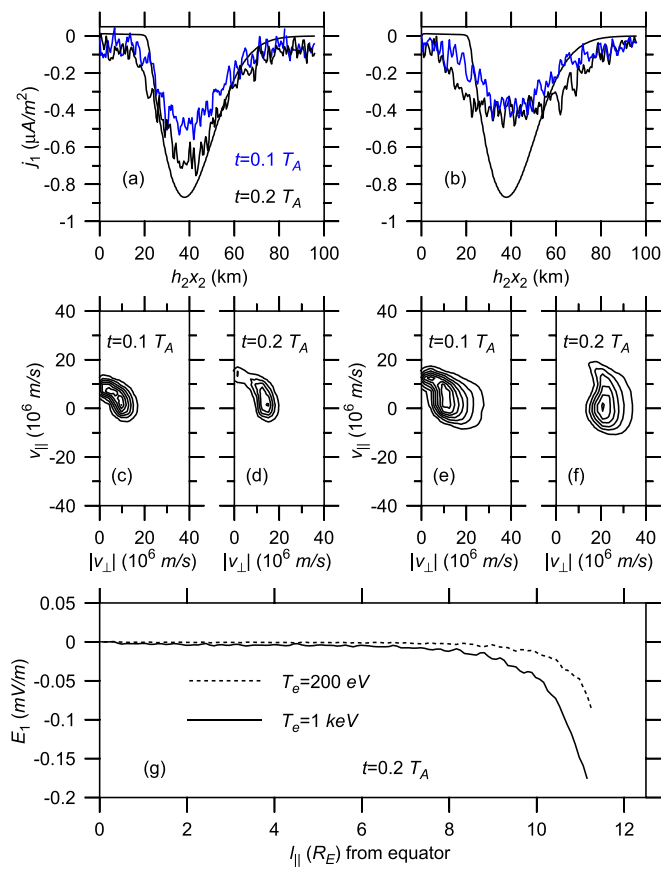

FIG. 2. The hybrid model parallel current, j_1, as a function of perpendicular distance across the simulation domain (h_2x_2) at the northern ionospheric boundary for (a) $T_e = 200$ eV and (b) $T_e = 1$ keV. Smooth black lines show the ideal MHD result. (c)+(d) Distribution function evolution at current maximum ($h_2x_2 = 38$ km) for $T_e = 200$ eV. (e)+(f) Distribution function evolution at current maximum for $T_e = 1$ keV. (g) Parallel electric field along the field line from the equator to the northern ionospheric boundary at the position of the current maximum ($h_2x_2 = 38$ km).

case with the extent of the broadening increasing with the temperature. The saturation and broadening was also noted in References 8 and 9 using the same simulation code.

The middle panels of Figure 2 display the distribution function (at the position of the current maximum) for the same times as the plots in Figures 2(a) and 2(b) (where in these figures, $v_{||}$ is the parallel electron velocity, v_1, and $v_\perp$ is the gyroaveraged perpendicular electron velocity[7]). The effect of the mirror force on the electron dynamics is clear from the ring distributions which result as some of electrons, accelerated to carry the field aligned current, undergo mirroring and travel back up the field line (as also noted in self-consistent simulations of Alfven wave pulse propagation, e.g., Ref. 12). The radius of the ring is larger in the $T_e = 1$ keV case because for larger temperatures, a larger fraction of electrons experience a mirror force sufficiently strong to overcome the accelerating potential and be reflected back up the field line. The remaining downward propagating population must, therefore, be accelerated more to carry the field aligned current. The gradual depletion of electrons at small pitch angles (particularly in the $T_e = 1$ keV case) coincides with a further broadening of the parallel current profile from $t = 0.1\ T_A$ to $t = 0.2\ T_A$.

The need to accelerate more trapped electrons in the keV case to carry the current, requires a correspondingly larger parallel electric field than the 200 eV case as illustrated in Figure 2(f), which plots the parallel electric field along the field line at the position of the current maximum ($h_2x_2 = 38$ km in Figure 2(a)). Although the current is reduced in the keV case, the mirror force effects still result in a significantly larger parallel electric field (relative to the 200 eV case), which is capable of accelerating electrons to observed keV energies.[9]

The dispersion of wave energy across magnetic field lines has long been associated with electron inertial and kinetic Alfvén wave limits where the presence of E_1 implies perpendicular Poynting flux ($S_2 = -E_1 b_3$), which propagates wave energy across magnetic field lines. However, in a system dominated by mirror force effects, the driving force for generating E_1 is different, but the net effect is the same. In order to separate whether the dispersion seen in the hybrid simulations is simply associated with the magnitude of this E_1 and not with any other wave-particle interaction, we revisit the broadening evident in Figure 2 with the MHD model described in Sec. II. In order to choose values for the conductivity, we appeal to the Knight relation[11] which is a current-voltage relation satisfied by a Maxwellian distribution of adiabatic electrons passing through a static potential drop in a nonuniform magnetic field (thus modeling the resistance of the mirror force). For a wide range of auroral parameters, this relation is linear and can be approximated by the function

$$j_1 = -K\Delta\phi, \tag{6}$$

where $\Delta\phi$ is the potential drop along the field line and $K = ne^2/\sqrt{2\pi m_e k_B T_e}$. The approximate consistency between the linear Knight relation and the current-voltage relation evident in the hybrid simulation for smaller values of $\Delta\phi$

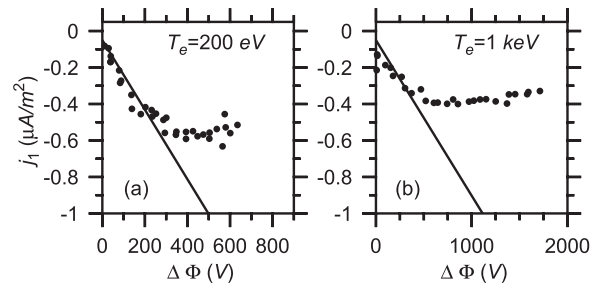

FIG. 3. Current-Voltage (C–V) relation along $h_2x_2 = 38$ km field line (calculated from hybrid simulation data) along with the corresponding solution of the linear Knight relation (solid line) for (a) $T_e = 200$ eV and (b) $T_e = 1$ keV. Note: intercept of solid lines have been chosen to best intersect hybrid simulation data in panel (a).

(due to the low frequency nature of the wave) was established in Reference 8. We repeat that analysis here, where Figure 3 displays the current voltage relationship as determined from the hybrid simulations by integrating the parallel electric field along the field line of current maximum ($h_2x_2 \approx 38$ km) from the equator to the ionospheric boundary

$$\Delta\phi = -\int_0^{l_{ionosphere}} dl E_1, \tag{7}$$

and plotting the potential drop against the parallel current at the ionospheric boundary. As with the Reference 8 study, there is a correspondence between the current-voltage relationship in the model and the Knight relation until the model current starts to saturate. Therefore, we confine our analysis to the lower current amplitudes at early times. Additional comment on the saturation will be given later.

Starting with Eq. (7), and substituting in for the parallel electric field using the parallel resistive Ohm's law (assuming constant density along the field line so that parallel current is only dependent on the magnetic field), the following formula, relating parallel potential drop and parallel current, can be derived

$$\Delta\phi = -\frac{1}{\sigma}(x_1 h_1)_{ionosphere} j_{1_{ionosphere}}, \tag{8}$$

so the relevant conductivity σ can be determined from the linear Knight coefficient, K, for a specific electron density and temperature by

$$\frac{1}{\sigma} = \frac{1}{K(h_1 x_1)_{ionosphere}}. \tag{9}$$

In Eqs. (8) and (9), the "ionosphere" subscript denotes the value of these variables at the northern ionospheric boundary. In determining σ from Eq. (9), the value of $(x_1 h_1)_{ionosphere}$ at $h_2x_2 = 38$ km was chosen, since this defines the position of the current maximum as illustrated in Figure 2.

The resulting ionospheric parallel current profiles from the resistive MHD simulations for $t = 0.15\ T_A$ are plotted in Figures 4(a) and 4(b) along with the hybrid solutions at the same time and the qualitative features of the broadening are

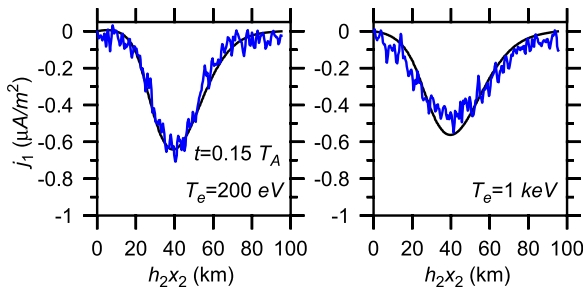

FIG. 4. Comparison of the parallel current profile, j_1, at northern ionospheric boundary between the resistive MHD (black lines) and hybrid (blue lines) models for (a) $T_e = 200$ eV and (b) $T_e = 1$ keV.

reproduced remarkably well. In contrast with the ideal MHD ($E_1 = 0$) results displayed in Figure 2, the drop in total current evident as T_e increases occurs because more wave energy is lost to the increased electron energization in the hybrid picture and to Ohmic dissipation (j_1E_1) in the MHD picture.

Consistent with previous comments, a plot of the perpendicular Poynting flux (Figure 5(a)) in the $T_e = 1$ keV case is substantially increased in magnitude and of wider perpendicular extent than the $T_e = 200$ eV case. The positive profile of S_2, in both cases, implies that wave energy is propagating from left to right in the figure, consistent with the decreasing steepness of the normalized azimuthal magnetic field profile (Figure 5(b)) as E_1 increases. This decrease in slope means that magnetic field energy is being transferred in the direction of increasing x_2 and also that the current layer is broader and weaker since $j_1 \propto \partial b_3/\partial x_2$. It should be noted as well that the Poynting flux is not only dispersing energy perpendicular to the magnetic field, but that this flux is feeding electron acceleration in the hybrid model and j_1E_1 ohmic dissipation in the resistive MHD picture.

The directionality of the perpendicular Poynting flux is a consequence of the perpendicular profile used in this study to isolate an upward current region. If a full Gaussian profile perpendicular to the magnetic field were used, both upward and downward current regions would result and energy would bi-directionally feed both current regions. If the perpendicular magnetic field profile were to change sign, then magnetic energy would be directed from both sides into the peak of the parallel current layer where it is dissipated.

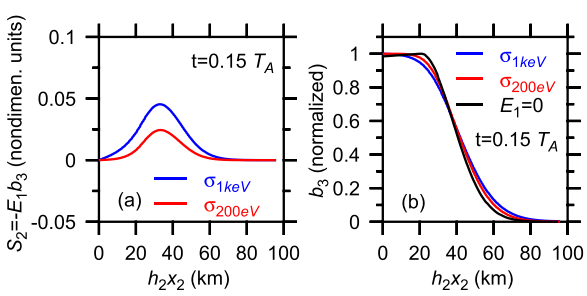

FIG. 5. (a) Perpendicular Poynting flux, $S_2 = -E_1b_3$ from the resistive MHD model at the northern ionospheric boundary. (b) Magnetic field from MHD model at the northern ionospheric boundary, normalized in order to emphasize the perpendicular scale length. σ_{T_e} is the conductivity calculated from Eq. (9) for the indicated value of T_e.

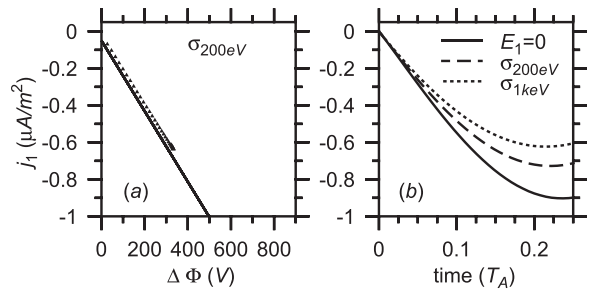

FIG. 6. (a) Current-voltage relationship from resistive MHD simulations for $\sigma_{200\text{eV}}$ (circles) as compared with the solution of the linear Knight relation for the same electron temperature. Note that the vertical offset is to facilitate comparison. (b) Maximum amplitude of the parallel current density, j_1, at the northern ionospheric boundary as a function of time for the ideal ($E_1 = 0$) and two resistive MHD simulations.

However, the perturbation would still broaden out in both directions at the edges.

Figure 6(a) plots the numerically determined current voltage relation from the $\sigma_{200\text{eV}}$ resistive MHD simulation along with the Knight solution for the same temperature confirming the analytical relation for σ (Eq. (9)). The numerical data, plotted for the interval from $t = 0$ to $t = 0.25\ T_A$, indicates that the parallel current density in this case reaches a maximum sooner than for the ideal MHD case ($E_1 = 0$). The same is true for the $\sigma_{1\text{keV}}$ case in Figure 6(b) where the maximum amplitude of the parallel current at the northern ionospheric boundary is plotted as a function of time for both the two resistive MHD cases and the ideal MHD case. It is clear from this figure that the reduced current maximum and broadening (as also evident in the hybrid simulations) is simply the result of the presence of the resistivity due to the parallel electric field. The divergence of the resistive MHD and hybrid systems over the longer term (Figure 3) is primarily due to the depletion of the availability of electrons at small pitch angles in the hybrid simulation which invalidates the description of the Knight relation and requires a more general approach that accounts for the differences in the parallel and perpendicular electron temperatures. This will be the focus of a future paper.

As mentioned previously, the perpendicular dispersion of wave energy is traditionally associated with the inertial and kinetic Alfvén wave limits. Of these two limits, electron inertial effects are important in the auroral acceleration region, above the ionospheric boundaries, where the parallel current density maximizes in these global modes. In Figure 7, we plot the ideal ($E_1 = 0$) and resistive MHD solutions along with an MHD solution incorporating electron inertial effects via the generalized Ohm's law given by

$$\frac{\partial}{\partial x_2}\left(\frac{h_3}{h_1h_2}\frac{\partial}{\partial x_2}(h_1E_1)\right) - \frac{h_1E_1}{\lambda_e^2} = \frac{\partial}{\partial x_2}\left(\frac{h_3}{h_1h_2}\frac{\partial}{\partial x_1}(h_2E_2)\right), \tag{10}$$

where the derivation in curvilinear coordinates can be found in Reference 7. It is clear that, for the parameters considered here, the dispersion associated with mirror force effects will dominate over that associated with electron inertial effects. This dominance of mirror force effects is simply due to the

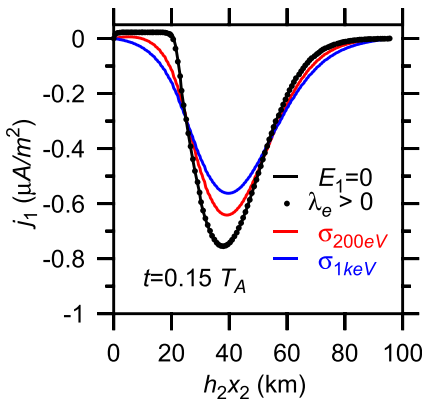

FIG. 7. Parallel current density, j_1, at the northern ionospheric boundary for the ideal and resistive MHD cases along with a new MHD case where electron inertial effects are considered.

fact that the contribution to E_1 from electron inertial effects is much smaller at these broad perpendicular scale lengths and thus there is less perpendicular Poynting flux to disperse wave energy.

As a final point, it is interesting to note that when the parallel Ohm's law is used along with Ampere's law in Eq. (2), the last term on the right-hand-side takes the form of a diffusion term in b_3 and thus the dispersion can also be interpreted to first order as a magnetic diffusion [e.g., Ref. 13] (as was noted for the case of anomalous resistivity effects by Reference 14). The consistency between the Poynting flux argument we have made here and magnetic diffusion is evident in a comparison of Figures 5(a) and 5(b) which illustrates that the width of the S_2 profile (panel a) is consistent with how the diffusion of magnetic energy from left to right broadens the steepness of the b_3 profile (panel b).

IV. CONCLUSIONS

Using a simplified MHD description, we have explained a perpendicular broadening of the parallel current profile that has appeared in hybrid MHD-kinetic electron simulations of the upward current region of global scale standing shear Alfvén waves along the Earth's closed magnetic field lines (also known as Field Line Resonances). The broadening increases with temperature in the hybrid system because mirror force effects ($\mu\nabla B$) dominate the parallel electric field generation. The same saturation and broadening of the field aligned current was also seen in resistive MHD simulations where the parallel Ohm's law was specified based on the linear Knight relation for the same electron temperatures and densities. This simplified description allows consideration of the broadening in the absence of other wave-particle interactions evident in the kinetic simulations. Therefore, the fact that the MHD results reproduces the general characteristics of the broadening evident in the hybrid model results confirms that $E_{||}$ associated with mirror force effects is driving the perpendicular dispersion. The increased $E_{||}$ facilitates increased perpendicular Poynting flux which in-turn propagates wave energy across magnetic field lines. This mirror force induced dispersion dominates over that associated with electron inertial effects for the parameters considered in this study. Additionally, although mirror force effects dominate the parallel electric field generation within the hybrid model, the MHD analysis is completely general, so any source of $E_{||}$ that can be effectively described by a resistive Ohm's law [e.g., Ref. 14] would lead to a similar dispersion.

ACKNOWLEDGMENTS

The authors acknowledge support from NASA grants (NNH09AM53I, NNH09AK63I and NNH11AR071) and NSF grants (ATM0902730 and AGS1203299) and DOE Contract DE-AC02-09CH11466.

[1]B. L. Xu, J. C. Samson, W. W. Liu, F. Creutzberg, and T. J. Hughes, J. Geophys. Res. **98**, 11531, doi:10.1029/93JA00435 (1993).
[2]W. Lotko, A. V. Streltsov, and C. W. Carlson, Geophys. Res. Lett. **25**, 4449, doi:10.1029/1998GL900200 (1998).
[3]J. C. Samson, R. Rankin, and V. T. Tikhonchuk, Ann. Geophys. **21**, 933 (2003).
[4]R. Rankin, J. C. Samson, and V. T. Tikhonchuk, Geophys. Res. Lett. **26**, 3601, doi:10.1029/1999GL010715 (1999).
[5]T. K. Nakamura, J. Geophys. Res. **105**, 10729, doi:10.1029/1999JA900494 (2000).
[6]R. L. Lysak and Y. Song, J. Geophys. Res. **108**, 1327, doi:10.1029/2003JA009859 (2003).
[7]P. A. Damiano, A. N. Wright, R. D. Sydora, and J. C. Samson, Phys. Plasmas **14**, 062904 (2007).
[8]P. A. Damiano and A. N. Wright, J. Geophys. Res. **113**, A09219, doi:10.1029/2008JA013087 (2008).
[9]P. A. Damiano and J. R. Johnson, Geophys. Res. Lett. **39**, L02102, doi:10.1029/2011GL050264 (2012).
[10]R. Lysak and W. Lotko, J. Geophys. Res. **101**, 5085, doi:10.1029/95JA03712 (1996).
[11]S. Knight, Planet. Space Sci. **21**, 741 (1973).
[12]C. E. J. Watt, R. Rankin, I. J. Rae, and D. M. Wright, Geophys. Res. Lett. **33**, L02106, doi:10.1029/2005GL024779 (2006).
[13]E. R. Priest, *Solar Magneto-hydrodynamics* (Dordrecht, Holland, Boston, D. Reidel Publications Co., Hingham, 1982).
[14]R. L. Lysak and C. T. Dum, J. Geophys. Res. **88**, 365, doi:10.1029/JA088iA01p00365 (1983).